Journal Homepage: -www.journalijar.com

INTERNATIONAL JOURNAL OF ADVANCED RESEARCH (IJAR)

Article DOI:10.21474/IJAR01/18949
DOI URL: http://dx.doi.org/10.21474/IJAR01/18949

RESEARCH ARTICLE

STUDY ON AUTOMATED DETECTION OF EQUATORIAL PLASMA BUBBLES EPB

Estelle Valérie Tapsoba[1], Doua Allain Gnabahou[1], Rolland Fleury[2] and Frédéric Ouattara[1]

1. Laboratoire de ChimieAnalytique de Physique Spatiale et Energétique (L@CAPSE), Université Norbert Zongo BP 376 Koudougou, Burkina Faso.
2. LAB-STICC, UMR 6285, Institut Mines-Telecom Atlantique, Brest, France.

Manuscript Info

Manuscript History
Received: 20 April 2024
Final Accepted: 24 May 2024
Published: June 2024

Key words:-
Equatorial Ionosphere, Sland Total Electron Content (STEC), Equatorial Plasma Bubbles (EPB)

Abstract

A processing application has been developed to detect and characterize localized plasma decreases: Equatorial plasma bubbles. The algorithm used is based on an automated search for negative STEC variations during a GPS satellite passage. First, an example of detection is shown. The method used has been applied to available data from seven (7) stations in West Africa, and the results over several years of measurements are presented. A study of spatial behavior was also carried out. The results show that the location of EPB bubbles depends on magnetic position. Bubbles are more present near the position of the North and South Equatorial Anomaly (EIA) ridges, but exist near the magnetic equator. Beyond 30° of inclination, bubbles are rarely present. The study of EPB characteristics also revealed durations mostly between 10 and 25 min, and maximum depths between 5 and 25 TECU.

Introduction:-

Equatorial Plasma Bubbles (EPB) are zones of lower plasma density. They are generated in the E layer of the ionosphere. This phenomenon occurs in the hours after sunset, when the production mechanism in the F layer continues, while that in the E layer is interrupted by rapid recombination. This creates a density difference between the upper surface of the E layer and the lower surface of the F layer. (McDonald et al., 2012; Woodman & La Hoz, 1976) explain that this local decrease in the density of the E-layer can give rise to a Rayleigh-Taylor (RT) instability at the origin of EPBs (C. Y. Huang et al., 2001; Kelley, 2009; Woodman & La Hoz, 1976).RT instability is mainly triggered by Pre-Reversal Enhancement (PRE), which corresponds to a change in current direction in the E region. Vertical drift of the plasma leads to a rise in the altitude of the bubbles created, which will also increase in amplitude (Bhattacharyya, 2022) EPBs can reach up to 1,500 km in altitude, and even higher in the equatorial region, as observed by coherent sounder measurements. Their size and depth in density vary according to season, local time of day and geographical location. Several authors (González, 2022; Li et al., 2020; Vankadara et al., 2022) have characterized EPB bubbles. (C. Y. Huang et al., 2001; C.-S. Huang, 2011; C.-S. Huang et al., 2014; Woodman & La Hoz, 1976) used coherent radar signal-to-noise and GPS measurements to study EPB occurrences. Ionosonde data have been used to establish the morphology of F-scattering. scattering morphology (Abdu et al., 1982, 2003, 2012; Carmo et al., 2021). These studies revealed that EPBs exhibit seasonal and geographical diurnal variation. Their presence is more pronounced in the nocturnal sector between sunset and midnight (Magdaleno et al., 2017a) have shown that the spatial variation of EPBs has a higher rate in the region around the magnetic equator. This rate decreases with distance from the equator. The presence of bubbles is as great in the longitude sector covering South America and West Africa (Magdaleno, Herraiz, et al., 2011a, 2011b; Barros et al., 2018).

Corresponding Author:- Doua Allain Gnabahou
Address:- Laboratoire de ChimieAnalytique de Physique Spatiale et Energétique (L@CAPSE), Université Norbert Zongo BP 376 Koudougou, Burkina Faso.

The study of EPBs is of great importance in the scintillation phenomenon. EPBs impact Earth-satellite systems with more or less rapid fluctuations in the phase and amplitude of the received radio signal. Scintillation is a phenomenon linked to irregularities in the ionospheric plasma. Africa, particularly in the West African zone, has a lack of data bases, which makes predictions difficult, and therefore constitutes a vast field to be explored. To make a better contribution to the study of plasma bubbles in the equatorial part of the West African zone, we present the GPS measurements used at several available stations. Next, we describe our algorithm for automated detection of plasma bubbles from phase-derived oblique total content measurements. Bubble characteristics are determined by the duration and maximum depth of sub-ionization. The analysis is performed as a function of the station's magnetic position. Our conclusion highlights the strong points obtained on the morphology of EPB bubbles in Africa.

Data

We used data from 07 stations in the IGS network, located in West Africa near the magnetic equator. The data used in this work are RINEX (Receiver INdependent Exchange) files clocked at 30 seconds and available on the CDDIS (Crustal Dynamics Data Information System) website at https://cddis.nasa.gov/archive/gnss/data/daily/. In Burkina Faso, a Novatel GSV ionospheric scintillator was installed as part of the IHY (International Heliophysical Year) project in November 2008. The station was added to our treatments. Figure 1 shows the geographical distribution of these 7 GPS stations. Three stations are close to the magnetic equator, while the other four are located on the northern and southern crests of the equatorial anomaly. The coordinates of the stations and their magnetic inclinations for 2010 and the range of years used are shown in Table 1.

Skewed total electron content (sTEC) measurements were estimated using the combination of phase measurements of the two frequencies L1 (1.57542 GHz) and L2 (1.22760 GHz) by eliminating the geometric term from the RINEX files.

Table 1:- List of stations used, positions and annual range of available data.

Station	Latitude Geographic	Longitude Geographic	Magnetic tilt	Measurementperiod
ASCG	-7.916	-14.333	-26.7	2015-2022
NKLG	0.354	9.672	-15.1	2001-2022
BJCO	6.752	2.265	-3.3	2009-2022
YKRO	6.871	-5.240	-2.9	2013-2022
KOUD	12.25	-2.37	8.0	2009-2022
DAKR	-14.68	17.465	14.9	2011-2020
CPVG	16.732	-22.935	20.1	2014-2022

Method:-

Our computer program rec_epb.m is the one developed and used to detect and characterize a plasma bubble from the time series of sTEC (s=slant) values derived from the phase (tec_phi). Phase measurements are less noisy (by a factor of around 10) than content obtained from code measurements (tec_code), and less sensitive to multipath at low elevations. Numerous works have been presented with a search for sTEC variations presenting well-characterized values over depth and duration (Blanch et al., 2018; Carmo et al., 2021; Kumar, 2017; Mersha et al., 2020; Vankadara et al., 2022) Our algorithm is based on a search for a particular form of the first derivative of the sTEC, taking inspiration from previous publications (Magdaleno et al., 2012; Portillo et al., 2008). We have opted for a simple and robust method, but whichcan lead to solutions that are not EPBs, as we shall seeitlater. Adding additional criteria (on the second driven in particular) would have eliminated false detections, but at the cost of more elaborate developments and possibly with losses of solutions (Magdaleno et al., 2013). We are aware that additional sorting is needed on the results provided by our method.

A plasma bubble corresponds to an always sub-ionized variation of the electronic content, i.e. with a period of decrease, a minimum value and an increase to reach a content level close to that before the bubble. On the first derivative, this temporal evolution corresponds to the shape of the 'integral' sign (∫) with a 'V' shape at the start of the sequence, a passage through 0 associated with the minimum value of the sTEC and an inverted 'V' shape in the positive variations. It is this particular shape that we have automatically searched for on the first derivative. The use of the first derivative with these few particular points brings much more robustness than the direct evolution of the STEC, and thus led us to our choice.

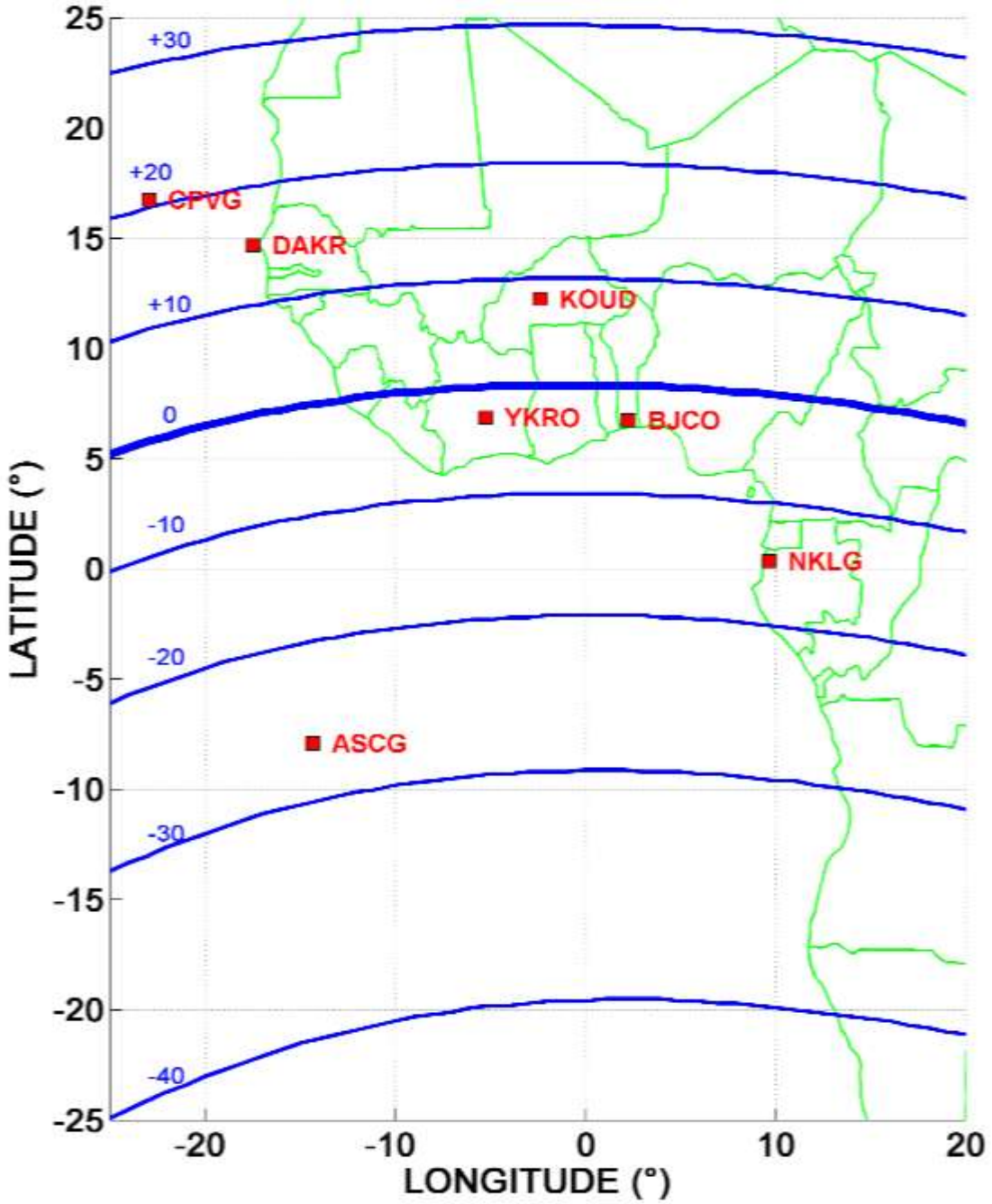

Figure 1:- The geographical positions of the 07 selected stations, the blue lines represent the different value of magnetic inclination (from +30 to -40; in 10 ° steps.

For each PRN run, we numerically calculate the first derivative of sTEC as the difference between two consecutive values, i.e. sTEC (t+30) minus sTEC (t).

$$\Delta \mathrm{sTEC} = \mathrm{sTEC}(t + 30) - \mathrm{sTEC}(t) \quad (1)$$

Then a sliding average over 12 points (360s) is calculated to eliminate the very short variations that don't correspond to the phenomenon we're looking for. We tested several smoothing lengths (270s ,360s ;720s) and the 360s length gave the best results. We chose to search only for bubbles of a certain size, so the first detection threshold was set at-60 tecu/h. . The passage of the derivative through 0 is memorized, as it corresponds to the instant of maximum bubble depth. The first derivative now becomes positive, and again we look for the instant of its passage to the value$+60$ tecu/h

$$-60 \text{ tecu/h} < threshold > 60 \text{ tecu/h} \quad (2)$$

Several thresholds were tested:80 tecu/h, 60tecu/h,40 tecu/h,, and the chosen one of ± 60 tecu/hcorresponds to the best visual solution on a few typical examples. At this stage, we haveidentified the 2 start (t1) and end (t2) instants of the bubble, and therefore its temporal duration. In figure2, the bubble's start and end times are indicated by arrows.

$$\mathbf{duration\ (mn)} = \mathbf{t_2 - t_1} \quad (3)$$

The process is iterated to search for new bubbles until the end of the PRN run. Many PRN runs take place over 2 consecutive days, but RINEX input files are daily, so incomplete detection of a bubble at the end of the day is lost.

The second piece of information used to characterize the bubble is its intensity, i.e. the extent of under-ionization. This is estimated on the vTEC vertical content (v=vertical). Knowing the 2 instants at which the bubble begins and ends, we perform a linear interpolation to obtain an estimated level at the minimum instant. The bubble depth is the difference between this estimate and the value obtained at minimum. The depth is shown in figure 2

$$\mathbf{depth = vTEC_m - vTEC_{min}} \quad \mathbf{(4)}$$

With $\mathbf{vTEC_m = vTEC_1 + (vTEC_1 - vTEC_2) \times \frac{t_{min} - t_1}{t_1 - t_2}}$ (5)

Having reached this stage in the description of our algorithm, it's important to note that we don't limit our bubble search to particular periods of time within a day. The application developed takes just a few minutes to process an entire year's worth of station data. All identified bubbles are archived in a txt file. The start () and end time () are expressed in hours, duration in minutes and depth in tecu. We have added additional information for processing the results: the day, the PRN number, the minimum local time (tl_min), the position of the Pierce IPP point (sublat, sublon) and the minimum elevation (elev).

To illustrate our algorithm and its descriptive text, we present an example of a graph (**Figure 2)** showing th**e** results of EPB equatorial bubble detection at the Koudougou station in 2014, a year located at the maximum of the SC#24 solar cycle. The curves are color-coded, with the sTEC in red, the first derivative in blue and the smoothed derivative in green. The beginning and end of the bubble are identified by vertical black lines. Between 2 consecutive lines, the black line corresponds to the linear interpolation used to calculate the depth.

Figure 2 corresponds to September 29, 2014 (date=272) on the PRN13 satellite. The first observation concerns the temporal evolution of STEC and its first derivative. While STEC slowly decreases and then increases after 2000 UT, the first derivative is highly variable, with oscillations of different amplitudes and periods. This figure justifies the number of points in our smoothing to eliminate short variations and retain only trends. Our detection algorithm therefore only works on the green curve.

With the threshold criterion at ± 60 tecu/h, we found a single bubble between hours 19.708 UT and 20.358 UT, a duration of 39 minutes. Its estimated depth is at 19.76 TL, corresponding to an elevation of 19.02°. Following this first bubble, we found 2 small possibilities on the STEC and its derivative, but of insufficient amplitude to be retained by our software.

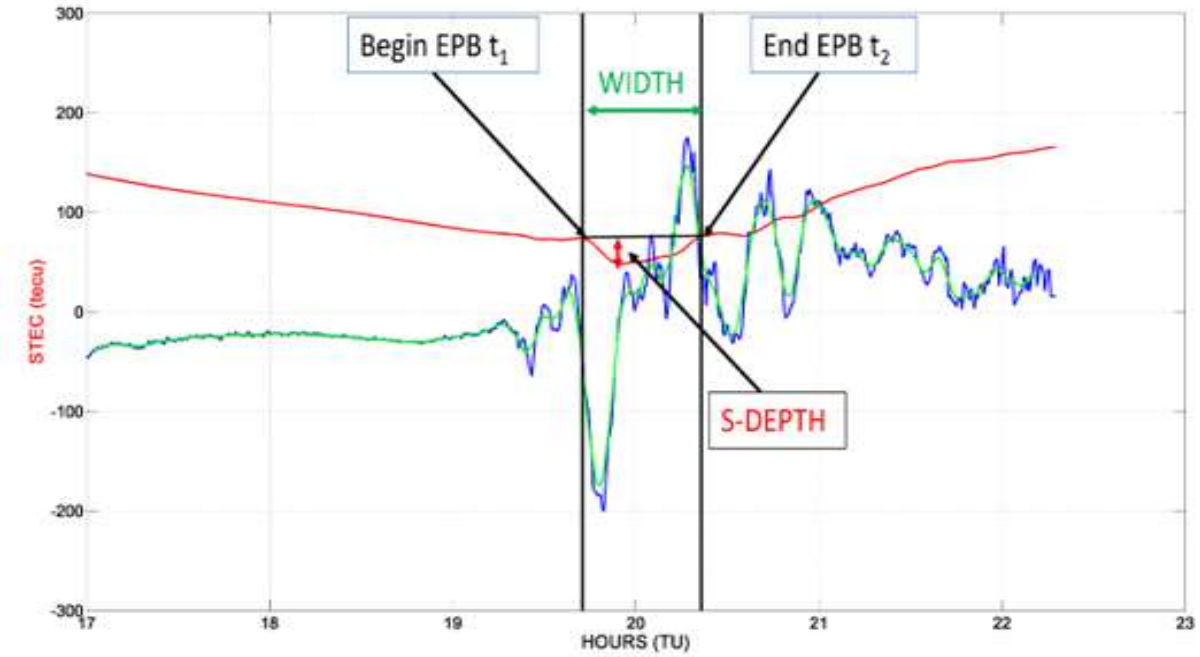

Figure 2:- Example of a single detection of an EPB bubble during a particular GPS pass

Result /Discussion:-

Geographical occurrence of EPB characteristics

The results obtained at the various stations have enabled us to present the characteristics of EPBs (trace and depth) in histograms, as shown in figure 3.

The histograms on the left (green) represent the number of EPB cases as a function of the duration between by steps of 1mn. The number of cases is normalized to the total number and is therefore expressed as a percentage, enabling us to compare histograms from different stations. The histograms on the right (red) represent the number of EPB cases as a function of maximum bubble depth. The number of cases is also expressed as a percentage in 1 tecu steps.

Figure 3:- Histogramma of the number of EPB detected as a function of duration (green) and depth (red) at Koud (upper panel) and NKLG (low paanel).

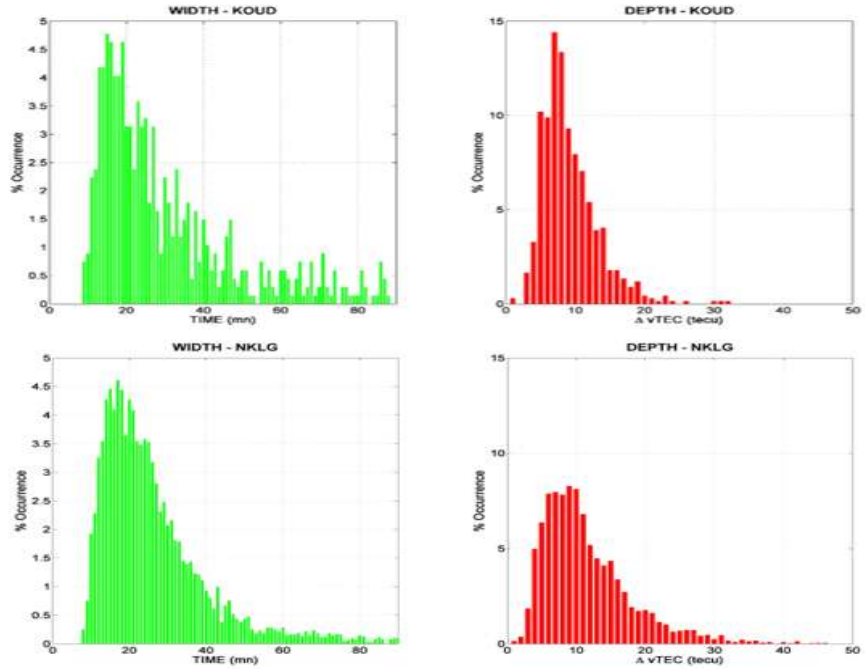

The normalized histograms obtained are similar for allthe seven (7) stations. We have therefore chosen to present only those stationsof KOUD and NKLG. The KOUD station has not yet been the subject of an EPB study, so the results obtained will be original. The second choice of NKLG is linked to its high availability, with 21 years of measurements enabling a good characterization of the phenomenon. The histograms have an asymmetrical Gaussian with a very rapid ascending phase and a slow decay phase, typical of an exponential. The maximum is between 10 and 20 min for duration and between 8 and 10 tecu for depth. Over 90% of EPBs detected have a duration of over 10 min. Beyond a typical value of 20 min duration, the distribution is more regular at NKLG and choppier at KOUD. This difference is certainly linked to the greater number of cases at NKLG, with twice as many years of measurements. Regarding the intensity of under-ionization, the percentage with a value greater than or equal to reaches 70% at KOUD, and around **90%** at NKLG. Occurrence is lower at KOUD, as it does not exceed the threshold of 20 tecu. On the other hand, there is a greater dispersion at NKLG, reaching slightly above 30 tecu. This difference may be linked to ambient density, with higher values at NKLG near the southern ridge, and lower values at KOUD on the equatorial edge of the northern ridge. The histograms obtained for the 5 other stations studied strongly resemble those of NKLG and do not call for any particular comment.

These results are in line with the work of several authors. Studies carried out in the African region show EPBs with depletion depths ranging from 05 tecu to 30 tecu (Abiriga et al., 2020; Portillo et al., 2008) with higher values recorded in stations located close to the Equatorial ionization anomaly peaks.

Geographical distribution of EPBs

In this section, we analyze the spatial variation in the occurrence of EPB bubbles. Figure 4 shows this variation for 9 stations (MAS1 and BKFP added to the original 7) for the 3 years 2013, 2014 and 2015 associated with the SC#24 solar cycle maximum.

For each station, we divided the geographical space into 4 quadrants: North-West, North-East, South-East and South-West. At the moment the bubble begins, we know the geographic coordinates of the Pierce IPP point, so we can position the bubble in its quadrant. To standardize the result once again, we calculated the percentage of points in relation to the sum of the points in the 4 quadrants, and plotted these figures on figure 4. For example, for the KOUD station, we obtained 47% of bubbles in the North-West quadrant and 12% in the North-East quadrant. The percentages to the south of the station are 26% for the west and 15% for the east.

In the Northern Hemisphere and the 3 stations furthest from the magnetic equator, there's a real asymmetry, with a higher percentage in the West than in the East. In the North/South direction, the percentage is higher in the two quadrants approaching the 20° magnetic inclination (upper blue line), which estimates the position of the northern equatorial ridge of the EIA anomaly. In particular, the figures for MAS1 are typical of this conclusion.

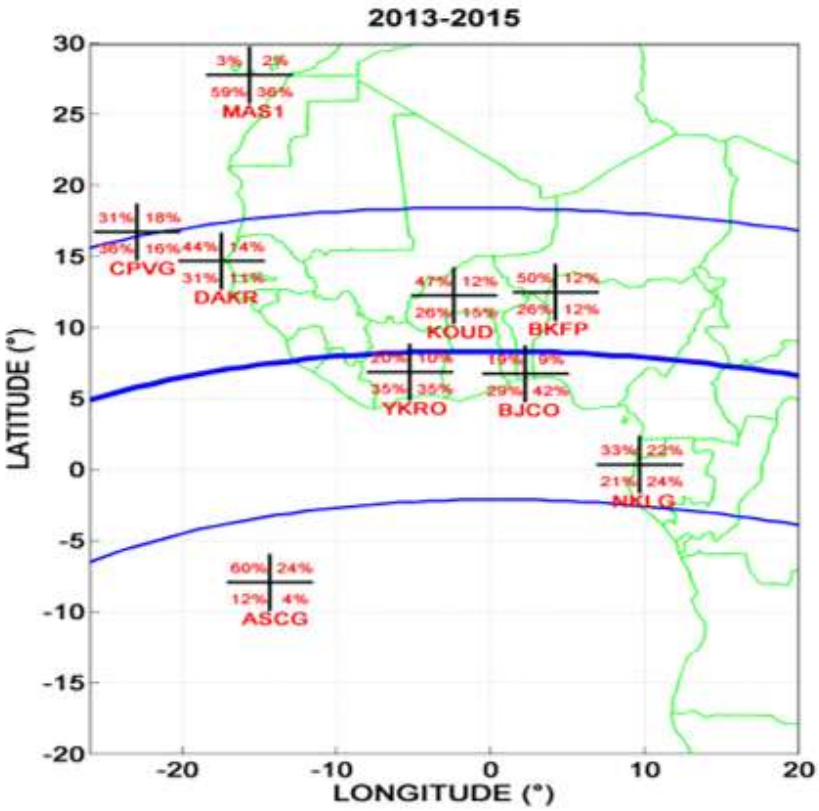

Figure 2:- Percentageof EPB in each quadrant over 3 years of measurements.

The 2 stations at KOUD and BKFP are geographically close, with identical rankings, so we can conclude that there is a good correlation at a distance of a thousand km in an east-west direction. Once again, the maximum percentage is obtained for the 2 northern squares. The 2 YKRO and BJCO stations are south of the magnetic equator (intermediate blue line) and this time, the maximum is for the 2 southern squares. BJCO is an exception, with a maximum in the East direction. The distribution is more balanced for the NKLG station, indicating a position certainly close to the southern crest of the EIA anomaly (lower blue line). Finally, the ASCG station, located furthest south in our network, confirms a maximum percentage towards the North, i.e. towards the South Ridge. As we approach the magnetic equator, the presence decreases, butitis not zero. The 2 MAS1 and ASCG stations are very close to the edge of the equatorial zone. Bubbles are more present to the west of the stations than to the east. This observation may be due to the presence of the South Atlantic Anomaly, which is a zone of strong scintillation. (Hammou Ali et al., 2021; C. Y. Huang et al., 2001;Magdaleno et al., 2017b). A future study taking into account stations in East Africa should confirm this conclusion.

Conclusion:-

We have developed an original method tofordetect EPBs on STEC time variations by working on the first derivative. The search is automated on RINEX files with 30s steps, and takes just a few minutes to process one year. Once the main parameters had been archived, we analyzed the results. Our software was applied to several low-latitude positions in West Africa. The bubbles obtained were identified by their duration and the depth of decay relative to the ambient environment. These parameters were analyzed in relation to the magnetic position of the stations.

The study of EPB characteristics showed that most of the EPB occurrences detected show an average decrease of 5 to 10 tecu and a duration between 10 and 25 min. Maximum EPB depths are between 5 and 25 tecu. The percentage of occurrences in terms of size and duration is higher at stations close to the magnetic equator.

Analysis of the results on the spatial behavior of EPBs showed that the distribution of EPBs depends on magnetic/geographic position. In the Northern Hemisphere, the highest percentages of bubbles are found to the north of the 4 stations (CPVG, DAKR, KOUD, BKFP). This means that the bubbles are located near the northern crest of the equatorial anomaly. There is a strong asymmetry between the 2 sectors, West and East, the origin of which we do not fully understand.

The 2 stations close to the south of the magnetic equator (YKRO and BJCO) have a greater distribution towards the south i.e. towards the southern crest of the EIA anomaly. The West/East asymmetry is less pronounced. The NKLG station confirms the balanced distribution around the South Ridge. The position of MAS1 and ASCG furthest from the magnetic equator confirms that the EPB phenomenon is localized in the equatorial zone, and decreases sharply beyond magnetic latitude ±25.

Bibliography:-

1. Abdu, M. A., Batista, I. S., Reinisch, B. W., MacDougall, J. W., Kherani, E. A., &Sobral, J. H. A. (2012). Equatorial range spread F echoes from coherent backscatter, and irregularity growth processes, from conjugate point digital ionograms. Radio Science, 47(06), 1-8.
2. Abdu, M. A., Batista, I. S., Takahashi, H., MacDougall, J., Sobral, J. H., Medeiros, A. F. de, & Trivedi, N. B. (2003). Magnetospheric disturbance induced equatorial plasma bubble development and dynamics : A case study in Brazilian sector. Journal of Geophysical Research: Space Physics, 108(A12).
3. Abdu, M. A., de Medeiros, R. T., &Sobral, J. H. A. (1982). Equatorial spread F instability conditions as determined from ionograms. Geophysical Research Letters, 9(6), 692-695.
4. Abiriga, F., Amabayo, E. B., Jurua, E., &Cilliers, P. J. (2020). Statistical characterization of equatorial plasma bubbles over East Africa. Journal of Atmospheric and Solar-Terrestrial Physics, 200, 105197. https://doi.org/10.1016/j.jastp.2020.105197
5. Barros, D., Takahashi, H., Wrasse, C. M., &Figueiredo, C. A. O. B. (2018). Characteristics of equatorial plasma bubbles observed by TEC map based on ground-based GNSS receivers over South America. Annales Geophysicae, 36(1), 91-100. https://doi.org/10.5194/angeo-36-91-2018
6. Bhattacharyya, A. (2022). Equatorial Plasma Bubbles : A Review. Atmosphere, 13(10), 1637. https://doi.org/10.3390/atmos13101637
7. Blanch, E., Altadill, D., Juan, J. M., Camps, A., Barbosa, J., González-Casado, G., Riba, J., Sanz, J., Vazquez, G., &Orús-Pérez, R. (2018). Improved characterization and modeling of equatorial plasma depletions. Journal of Space Weather and Space Climate, 8, A38.
8. Carmo, C. de S. do, Denardini, C. M., Figueiredo, C. A. O. B., Resende, L. C. A., Picanço, G. A. da S., Neto, P. B., Nogueira, P. A. B., Moro, J., & Chen, S. S. (2021). Evaluation of different methods for calculating the ROTI index over the Brazilian sector. Radio Science, 56(8), 1-12.
9. González, G. de L. (2022). Spread-F characteristics over Tucumán near the southern anomaly crest in South America during the descending phase of solar cycle 24. Advances in Space Research, 69(3), 1281-1300. https://doi.org/10.1016/j.asr.2021.11.009
10. Hammou Ali, O., Zaourar, N., Fleury, R., & Amory-Mazaudier, C. (2021). Transient variations of vertical total electron content at low latitude during the period 2013–2017. Advances in Space Research, 68(12), 4857-4871. https://doi.org/10.1016/j.asr.2021.02.039
11. Huang, C. Y., Burke, W. J., Machuzak, J. S., Gentile, L. C., & Sultan, P. J. (2001). DMSP observations of equatorial plasma bubbles in the topside ionosphere near solar maximum. Journal of Geophysical Research: Space Physics, 106(A5), 8131-8142.
12. Huang, C.-S. (2011). Occurrence of equatorial plasma bubbles during intense magnetic storms. International Journal of Geophysics, 2011.
13. Huang, C.-S., de La Beaujardiere, O., Roddy, P. A., Hunton, D. E., Liu, J. Y., & Chen, S. P. (2014). Occurrence probability and amplitude of equatorial ionospheric irregularities associated with plasma bubbles during low and moderate solar activities (2008–2012). Journal of Geophysical Research: Space Physics, 119(2), 1186-1199.
14. Kelley, M. C. (2009). The Earth's ionosphere : Plasma physics and electrodynamics. Academic press.
15. Kumar, S. (2017). Morphology of equatorial plasma bubbles during low and high solar activity years over Indian sector. Astrophysics and Space Science, 362(5), 93.
16. Li, Q., Zhu, Y., Fang, K., & Fang, J. (2020). Statistical Study of the Seasonal Variations in TEC Depletion and the ROTI during 2013–2019 over Hong Kong. Sensors, 20(21), 6200. https://doi.org/10.3390/s20216200

17. Magdaleno, S., Cueto, M., Herraiz, M., Rodríguez-Caderot, G., Sardón, E., & Rodríguez, I. (2013). Ionospheric bubbles detection algorithms: Analysis in low latitudes. Journal of Atmospheric and Solar-Terrestrial Physics, 95, 65-77.
18. Magdaleno, S., Herraiz, M., Altadill, D., & de la Morena, B. A. (2017a). Climatology characterization of equatorial plasma bubbles using GPS data. Journal of Space Weather and Space Climate, 7, A3.
19. Magdaleno, S., Herraiz, M., & de La Morena, B. A. (2012). Characterization of equatorial plasma depletions detected from derived GPS data in South America. Journal of atmospheric and solar-terrestrial physics, 74, 136-144.
20. Magdaleno, S., Herraiz, M., &Radicella, S. M. (2011a). Ionospheric bubble seeker : A Java application to detect and characterize ionospheric plasma depletion from GPS data. IEEE transactions on geoscience and remote sensing, 50(5), 1719-1727.
21. McDonald, S. E., Drob, D. P., Emmert, J., Englert, C., Siskind, D., Huba, J., Krall, J., &Basu, S. (2012). The importance of thermospheric winds for ionospheric modeling. A White Paper for the Decadal Survey of Solar and Space Physics.
22. Mersha, M. W., Lewi, E., Jakowski, N., Wilken, V., Berdermann, J., Kriegel, M., &Damtie, B. (2020). A method for automatic detection of plasma depletions by using GNSS measurements. Radio Science, 55(3), e2019RS006978.
23. Portillo, A., Herraiz, M., Radicella, S. M., &Ciraolo, L. (2008). Equatorial plasma bubbles studied using African slant total electron content observations. Journal of Atmospheric and Solar-Terrestrial Physics, 70(6), 907-917.
24. Vankadara, R. K., Panda, S. K., Amory-Mazaudier, C., Fleury, R., Devanaboyina, V. R., Pant, T. K., Jamjareegulgarn, P., Haq, M. A., Okoh, D., &Seemala, G. K. (2022). Signatures of Equatorial Plasma Bubbles and Ionospheric Scintillations from Magnetometer and GNSS Observations in the Indian Longitudes during the Space Weather Events of Early September 2017. Remote Sensing, 14(3), 652. https://doi.org/10.3390/rs14030652
25. Woodman, R. F., & La Hoz, C. (1976). Radar observations of F region equatorial irregularities. Journal of Geophysical Research, 81(31), 5447-5466.